

1 **Supplemental ~~Information~~ Materials For:**  
2 **Fine Particle Mass Monitoring with Low-Cost Sensors: Corrections**  
3 **and Long-Term Performance Evaluation**

4 Carl Malings<sup>1,2</sup>, Rebecca Tanzer<sup>1</sup>, Aliaksei Hauryliuk<sup>1</sup>, Provat K. Saha<sup>1</sup>, Allen L. Robinson<sup>1</sup>,  
5 Albert A. Presto<sup>1</sup>, R-Subramanian<sup>1,2</sup>

6 <sup>1</sup>Center for Atmospheric Particle Studies, Carnegie Mellon University, 5000 Forbes Avenue,  
7 Pittsburgh, PA 15213. Email: [subu@cmu.edu](mailto:subu@cmu.edu) (Corresponding Author)

8 <sup>2</sup>[OSU-EFLUVE, CNRS, Université Paris-Est Créteil, 61 Avenue du Général de Gaulle, 94000](#)  
9 [Créteil, France](#)

10 This document contains information meant to supplement and support the information presented  
11 in the paper referenced above. Section S.1 provides pictures of the RAMP sensor and associated  
12 PM sensors. Section S.2 describes the method for computing hygroscopic growth factors and  
13 investigates the sensitivity of these factors to changes in aerosol composition. Section S.3  
14 provides details on how empirical correction methods were selected. Section S.4 outlines the  
15 methods proposed for sensor drift adjustment, and provides results relating to these methods.  
16 Section S.5 provides formulae for the assessment metrics presented in this paper. Section S.6  
17 presents data collected on particle size distributions in Pittsburgh. Section S.7 presents various  
18 results providing further details about the performance of various correction approaches applied  
19 to low-cost PM sensor data. Finally, Section S.8 provides a figure depicting the results related to  
20 the short-term use case assessment of the low-cost sensors.

Formatted: Justified

21 **S.1. RAMP and PM Sensor Picture**



22  
23 Figure S.1: Several RAMP monitors (red boxes) with connected Met-One NPM (yellow box)  
24 and PurpleAir (purple box) PM<sub>2.5</sub> sensors.

25 **S.2. Correction Methods – Hygroscopic Growth Factor Computation**

26 This hygroscopic growth factor is computed as:

27 
$$fRH(T, RH) = 1 + \kappa_{\text{bulk}} \frac{a_w(T, RH)}{1 - a_w(T, RH)} \quad (\text{S.1})$$

28 where:

29 
$$a_w(T, RH) = RH \exp\left(\frac{4\sigma_w M_w}{\rho_w R T D_p}\right)^{-1} \quad (\text{S.2})$$

30  $\kappa_{\text{bulk}}$  is the hygroscopicity of bulk aerosol;  $\kappa_{\text{bulk}} = \sum_i x_i \kappa_i$  where  $x_i$  and  $\kappa_i$  are the volume  
31 fraction hygroscopicity parameters of the  $i^{\text{th}}$  component comprising the particle. Organic,  
32 sulfate, nitrate and ammonium are assumed as the main components comprising the particle. The  
33 fractional contributions of these chemical components to PM<sub>2.5</sub> during summer, winter, and as an  
34 annual average (applied to other periods) are obtained from recent AMS measurements in  
35 Pittsburgh (Gu et al. 2018) and their hygroscopicity parameters are adopted from literature  
36 (Cerully et al. 2015; Petters and Kreidenweis 2007).  $a_w$  is the water activity parameter, estimated  
37 using Eq. (S.2), where  $\sigma_w$ ,  $M_w$ , and  $\rho_w$  represent the surface tension, molecular weight and  
38 density of water, respectively;  $T$  is the absolute temperature,  $R$  is the ideal gas constant,  $RH$  is  
39 ambient relative humidity;  $D_p$  is the particle diameter, adopted as volume median diameter from  
40 long-term size distribution measurements using SMPS in Pittsburgh. Table S.1 lists different  
41 parameter values used in hygroscopic growth factor calculation.

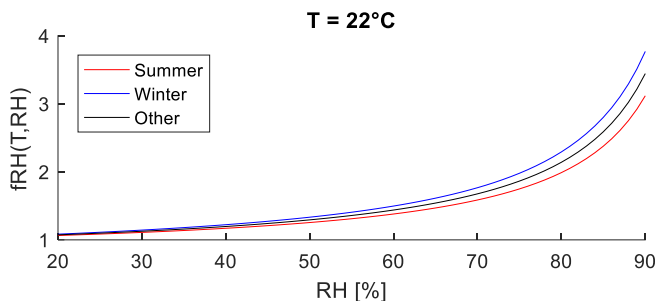
42

Table S.1: Parameters used in hygroscopic growth factor calculation

Parameter	Value			Unit	Source
	Summer	Winter	Other		
$\kappa_{OA}$	0.15	0.15	0.15	-	(Cerully et al. 2015)
$\kappa_{SO4}$	0.5	0.5	0.5	-	(Petters and Kreidenweis 2007)
$\kappa_{NO3}$	0.6	0.6	0.6	-	(Petters and Kreidenweis 2007)
$\kappa_{NH4}$	0.5	0.5	0.5	-	(Petters and Kreidenweis 2007)
$x_{OA}$	0.64	0.41	0.53	-	(Gu et al. 2018)
$x_{SO4}$	0.24	0.16	0.20	-	(Gu et al. 2018)
$x_{NO3}$	0.04	0.29	0.165	-	(Gu et al. 2018)
$x_{NH4}$	0.08	0.15	0.115	-	(Gu et al. 2018)
$\kappa_{bulk}$	0.26	0.34	0.30	-	
$\sigma_w$	0.072	0.072	0.072	N/m	
$M_w$	0.018	0.018	0.018	kg/mol	
$\rho_w$	1000	1000	1000	kg/m <sup>3</sup>	
$R$	8.314	8.314	8.314	J/mol K	
$D_p$	200	200	200	nm	

Field Code Changed  
 Field Code Changed  
 Field Code Changed  
 Field Code Changed

43



44

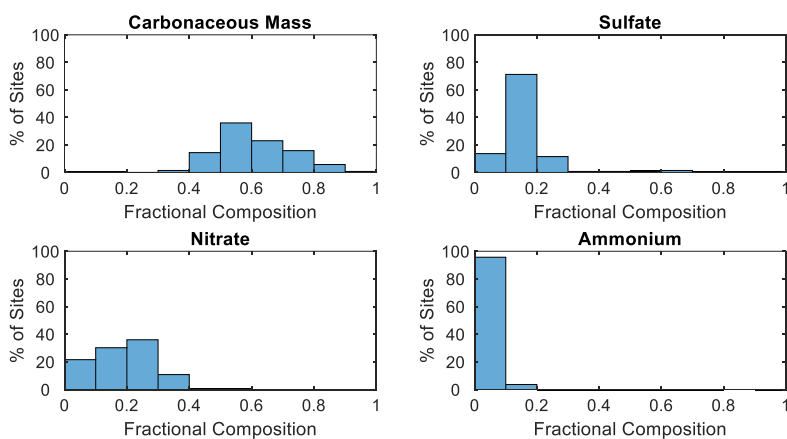
Figure S.2: Example of how the hygroscopic growth factor varies with humidity in summer, winter, and otherwise.

45  
46

47 To examine the sensitivity of the hygroscopic growth factor to different aerosol compositions, a  
 48 sensitivity analysis was conducted for differing aerosol compositions resulting in different  $\kappa_{bulk}$   
 49 values. Using data from the EPA Chemical Speciation Network for 2018 (available online at  
 50 [https://aq5.epa.gov/aq5web/airdata/download\\_files.html](https://aq5.epa.gov/aq5web/airdata/download_files.html)), the fractional composition of PM<sub>2.5</sub> as  
 51 carbonaceous matter, sulfate, nitrate, and ammonium were determined, and annual average bulk  
 52 hygroscopicity factors were computed for each of 139 sites where these data are available.  
 53 Carbonaceous mass was computed using a sum of elemental carbon and organic mass (OM,  
 54 calculated as organic carbon multiplied by 1.8) (Turpin and Lim 2001). The  $\kappa$  value for EC was  
 55 assumed the same as for OM; EC was typically from 8% to 18% of OM, so errors due to this

Formatted: Subscript

56 assumption should be small. Histograms for the fractional composition of these components  
57 across network sites are presented in Figure S.3.



Formatted: Keep with next

58

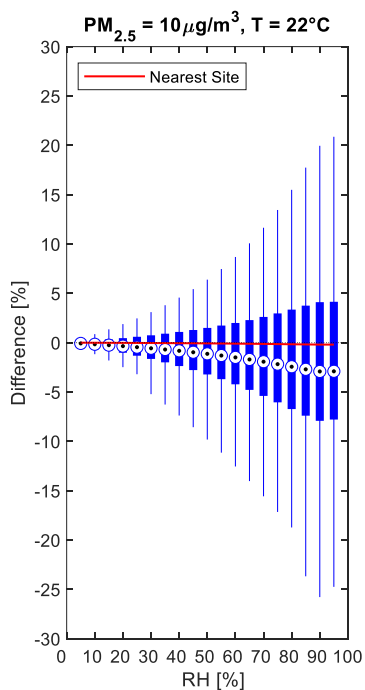
59 Figure S.3: Histograms representing the ranges in fractional compositions for carbonaceous,  
60 sulfate, nitrate, and ammonium components of PM<sub>2.5</sub> measured at 139 sites in the US EPA  
61 Chemical Speciation Network.

Formatted: Subscript

62 Figure S.4 presents the results as a function of relative humidity (in five percentage point  
63 increments), for a base concentration of 10  $\mu\text{g}/\text{m}^3$  at an ambient temperature of 22°C. The  
64 boxplots indicate the spread (across the speciation network sites) of the percent difference  
65 between PM readings corrected using each of the 139 speciation sites and PM readings corrected  
66 using the Pittsburgh values of  $\kappa_{\text{bulk}}$ , as determined from the AMS data and presented in Table  
67 S.1. The solid black line indicates results when using only the nearest speciation site to  
68 Pittsburgh outside of Allegheny county (in Washington county, about 35 km away). Overall, the  
69 failure to use an appropriate local  $\kappa_{\text{bulk}}$  factor typically (i.e. for the interquartile range of site  
70 compositions) causes less than 10% errors and may lead to up to 25% errors in extreme cases.  
71 However, using a nearby local factor, errors can be reduced below 1%. Therefore, it is  
72 recommended to use speciation information from the closest available station if specific local  
73 information is not available. It should further be noted that these results all employ the same  
74 linear correction coefficients from Eq. (3) as were determined for Pittsburgh, as presented in  
75 Table 1; if local collocations are performed to determine appropriate coefficients for each area,  
76 the resulting errors are likely to be further reduced or eliminated. Furthermore, while PM  
77 composition and size distribution at a given location may change significantly from day-to-day  
78 (Saha et al. 2019), the settings used in the proposed corrections reflect long-term averages. Thus,  
79 while they cannot capture such short-term fluctuations (as is reflected by the residual uncertainty  
80 in the presented results), they provide more robust performance in the long-term without the

Field Code Changed

81 need for simultaneous composition and size distribution information to be collected alongside  
82 low-cost sensor data.



Formatted: Not Highlight

Formatted: Figure, Indent: Left: 0"

83

84 Figure S.4: Sensitivity analysis of hygroscopic growth rate corrections. Boxplots indicate the  
85 range of percent differences between corrections performed using each of the chemical  
86 compositions measured at sites in the EPA Chemical Speciation Network and corrections  
87 performed using the Pittsburgh chemical composition (as described above). Results are binned  
88 by relative humidity. The solid red line indicates the percent differences from using chemical  
89 composition data at the nearest non-Pittsburgh site.

Field Code Changed

Formatted: Not Highlight

90

Formatted: Normal, Indent: Left: 0"

91 Several explanatory factors were considered for the empirical correction method. Dewpoint  $DP$   
92 was considered as a factor related to condensation that might serve as a proxy for the  
93 hygroscopic growth factor which is independent of aerosol composition. Furthermore, humidity  
94 is known to affect the performance of optical particle sensors directly (e.g. Jayaratne et al. 2018),  
95 and so relative humidity  $RH$  was included as a factor. Finally, temperature  $T$  was included as a

Field Code Changed

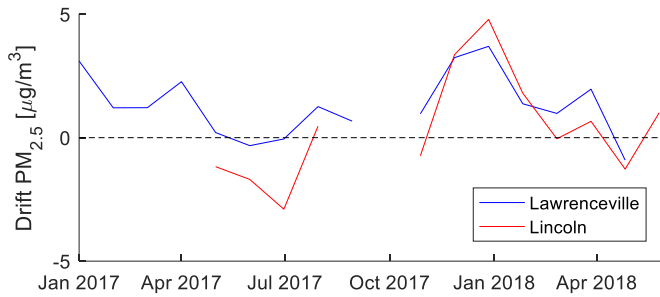
96 factor since it has been observed to affect the performance of optical sensor components  
97 (Johnson et al. 2016; Jayaratne et al. 2018; Zheng et al. 2018).

Field Code Changed

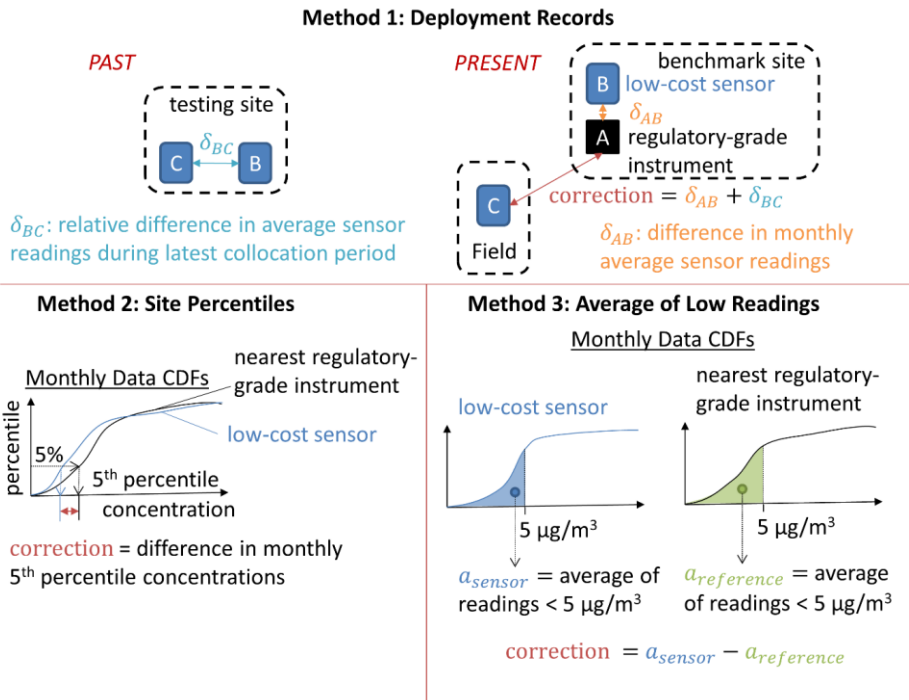
98 Various combinations of the as-reported sensor readings and the above inputs into various  
99 functional forms and with different application thresholds were applied to generate correction  
100 equations. Two functional forms were considered: linear and quadratic regression models.  
101 Thresholds were considered to define different subsets of the domain over which different  
102 functional parameters could be applied, allowing for piecewise-linear or piecewise-quadratic  
103 functions. Models without thresholds were considered, as well as models with single or multiple  
104 threshold values chosen from among 5, 10, 15, 20, 30, 40, and 50  $\mu\text{g}/\text{m}^3$  (as determined from the  
105 raw sensor reading). For reference, ambient concentrations in Pittsburgh typically range from 3  
106 to 20  $\mu\text{g}/\text{m}^3$ .

107 Models were calibrated using a combination of data collected at both the Lawrenceville and  
108 Lincoln sites from half of the sensors deployed to each site (the “training” set); model  
109 performance was evaluated on the other half of sensors at these sites (the “testing” set).  
110 Performance metrics assessed for the various models are included as supplementary data. The  
111 performance of each correction model on the test sensor set was scored using a heuristic  
112 combining various performance metrics (bias, mean absolute error, r, and threshold classification  
113 score) across a range of concentrations experienced at both collocation sites and penalizing the  
114 complexity of the model (and therefore its propensity to overfit to training data). The format of  
115 this scoring system was inspired by the “Eureka” equation discovery system of Schmidt and  
116 Lipson (2009), with modifications for the specific context of this problem (see the supplementary  
117 data for the resulting metrics). The resulting metrics are available in a table attached to the  
118 supplementary materials but separate from this document.~~For selecting a final correction method~~  
119 ~~for each type of sensor, performance across a range of concentrations experienced at both~~  
120 ~~collocation sites was traded off against the complexity of the model (and therefore its propensity~~  
121 ~~to overfit to training data).~~

122 **S.5.S.4. Drift-Adjustment Methods**

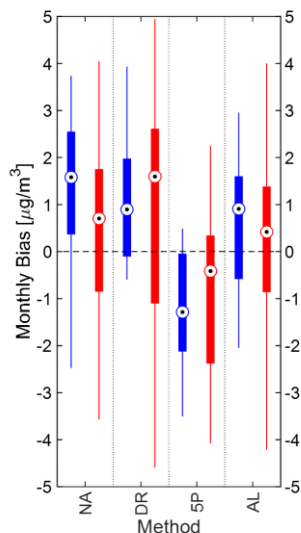


123  
124 Figure S.53: Illustration of observed NPM sensor drift at the Lincoln and Lawrenceville sites.  
125 Drift is depicted as the difference in monthly average readings of the NPM sensor, corrected  
126 using Eq. (4), versus the collocated regulatory-grade instrument at each site.



127  
128 Figure S.64: Diagrams of the three proposed drift-adjustment methods.

129 Note that in the Average of Low Readings method, if no readings within a month are below 5  
 130 micrograms per cubic meter, the minimum reading for that month is instead used as the basis for  
 131 the adjustment.



132  
 133 Figure S.7: Performance of various drift-adjustment methods in reducing the bias in monthly  
 134 averages; NA – no adjustment applied; DR – drift-adjusted using deployment records; 5P –  
 135 drift-adjusted using percentiles of nearest reference site; AL – drift-adjusted using averages of  
 136 low readings at nearest reference site. Performance is determined separately for the NPM  
 137 instruments deployed for extended periods at the Lawrenceville (blue) and Lincoln (red) sites.  
 138 Corrections are performed using Eq. (4).

139 Figure S.7 shows the spread in monthly biases (difference between the monthly average readings  
 140 of the corrected sensors and the BAM instruments) for both long-term collocation sites, both  
 141 without drift-adjustment and with the three proposed drift-adjustment methods. Note that these  
 142 biases are for the single long-term-deployment sensor at each site, whereas Figure 5 in the main  
 143 paper presented results for the entire “testing” set of sensors over a shorter period.

#### 144 **S.6.S.5. Assessment metrics**

145 For  $n$  measurements of concentration by the sensor ( $c$ ) and reference ( $\hat{c}$ ), bias is computed as:

146 
$$\text{bias} = \frac{1}{n} \sum_{i=1}^n (c_i - \hat{c}_i) \quad (\text{S.3})$$

147 mean absolute error (MAE) is evaluated as:

$$148 \quad \text{MAE} = \frac{1}{n} \sum_{i=1}^n |c_i - \hat{c}_i| \quad (\text{S.4})$$

149 and the Pearson correlation coefficient ( $r$ ) is evaluated as:

$$150 \quad r = \frac{\sum_{i=1}^n (c_i - \frac{1}{n} \sum_{j=1}^n c_j) (\hat{c}_i - \frac{1}{n} \sum_{j=1}^n \hat{c}_j)}{\sqrt{\sum_{i=1}^n (c_i - \frac{1}{n} \sum_{j=1}^n c_j)^2} \sqrt{\sum_{i=1}^n (\hat{c}_i - \frac{1}{n} \sum_{j=1}^n \hat{c}_j)^2}} \quad (\text{S.5})$$

151 These statistics assess, respectively, the systematic differences between the sensor and reference  
152 measurements over time, the average absolute difference in measurements taken at the same  
153 time, and the degree of linearity between the measurements. Lower absolute values of bias and  
154 MAE denote better agreement, while a value of  $r$  close to 1 denotes stronger correlation.

155 Additionally, the following EPA bias and precision score metrics (Camalier et al.  
156 2007)(Camalier et al., 2007) were used:

$$157 \quad \text{Precision Score} = \frac{n \sum_{i=1}^n \delta_i^2 - (\sum_{i=1}^n \delta_i)^2}{n \chi_{0.1, n-1}^2} \quad (\text{S.6})$$

158 where  $\chi_{0.1, n-1}^2$  denotes the 10<sup>th</sup> percentile of the chi-squared distribution with  $n - 1$  degrees of  
159 freedom, and:

$$160 \quad \delta_i = 100 \frac{c_i - \hat{c}_i}{\hat{c}_i} \quad (\text{S.7})$$

161 The bias score is:

$$162 \quad \text{Bias Score} = \frac{1}{n} \sum_{i=1}^n |\delta_i| + \frac{t_{0.95, n-1}}{n} \sqrt{\frac{n \sum_{i=1}^n \delta_i^2 - (\sum_{i=1}^n |\delta_i|)^2}{n-1}} \quad (\text{S.8})$$

163 where  $t_{0.95, n-1}$  is the 95<sup>th</sup> percentile of the t distribution with  $n - 1$  degrees of freedom. These  
164 precision and bias scores can be compared to performance guidelines for various sensing  
165 applications (Williams et al. 2014)(Williams et al., 2014). For PM<sub>2.5</sub>, requirements for  
166 educational monitoring (Tier I) are for precision and bias scores below 50%; for hotspot  
167 identification and characterization (Tier II) or personal exposure monitoring (Tier IV), these  
168 should be below 30%; for supplemental monitoring (Tier III), below 20%; and for regulatory  
169 monitoring (Tier V), below 10%.

## 170 **S.7-S.6. Seasonal Changes in PM<sub>2.5</sub> fraction below 300 nm in Pittsburgh**

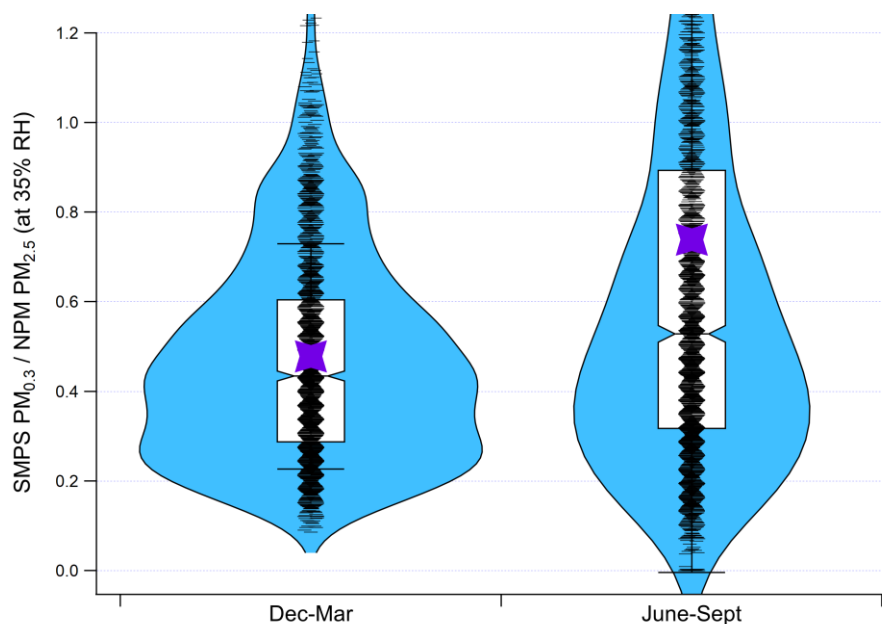
171 Aerosol size distributions over the 10-300 nm mobility size range were measured with a TSI  
172 scanning mobility particle sizer (SMPS) at the CMU campus. PM<sub>0.3</sub> mass concentrations were  
173 estimated assuming a mobility density of 1 gm/cm<sup>3</sup> and spherical particles, and then corrected to

Field Code Changed

Field Code Changed

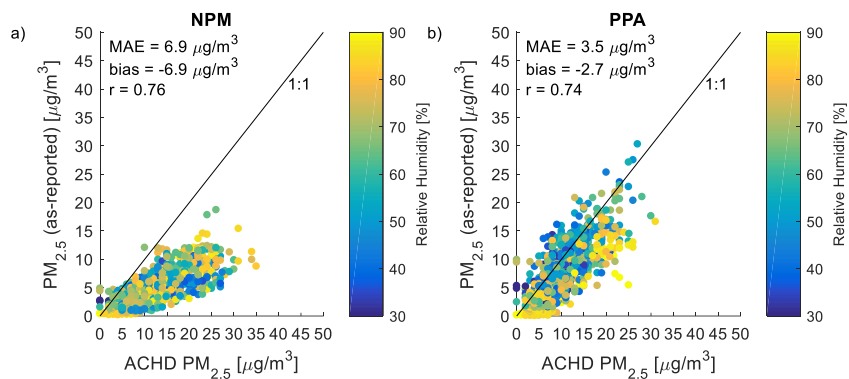
174 the equivalent mass at 35% RH using the previously-discussed hygroscopic corrections.  $PM_{2.5}$   
 175 mass concentrations were obtained from an NPM instrument attached to a RAMP co-located  
 176 with the SMPS. These values were corrected using Eq. (43). For the winter months, the RAMP  
 177 RH was assumed to be the same as the conditions inside the SMPS. For the summer months, we  
 178 assumed that the SMPS RH was 15% higher (than the RAMP RH) inside the air-conditioned  
 179 trailer where the SMPS operated. The SMPS/NPM comparison is further complicated by the fact  
 180 that we are comparing an electrical mobility sizer to an optical sizer, but the overall result of  
 181 higher sub-300 nm aerosol mass is consistent with previously reported results. [Stanier et al.](#)  
 182 [\(2004\) observed a larger aerosol volume in the 100-560 nm size range in the summer months](#)  
 183 [during the 2001-2002 Pittsburgh Air Quality Study. Saha et al. \(2018\) found that in 2016-2017,](#)  
 184 [though  \$SO\_2\$  concentrations have reduced compared to 2001-2002 resulting in fewer nucleation](#)  
 185 [events, the warmer months still see higher frequency of nucleation events and with higher](#)  
 186 [intensity compared to the winter months.](#)

Formatted: Subscript



187  
 188 Figure S.85: Ratios of  $PM_{0.3}$  to  $PM_{2.5}$  based on summer and winter data collected in Pittsburgh.  
 189 Individual data points are jittered; means are shown by the purple stars; whiskers represent one  
 190 standard deviation of the data. Values greater than unity likely indicate data where our  
 191 assumptions are no longer valid, but these are <25% of the data. The median  $PM_{0.3}/PM_{2.5}$  is 0.43  
 192 in the winter and 0.53 in the summer. For an annual average concentration of  $\sim 10 \mu g/m^3$ , this  
 193 represents a  $1 \mu g/m^3$  higher sub-300 nm fraction in the summer.





203

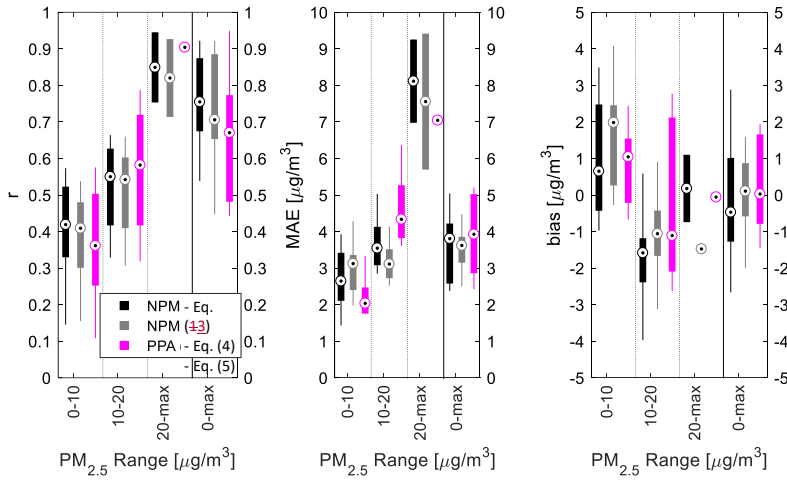
204 Figure S.96: Comparison of median one-hour-average NPM (a) and PPA (b) sensor readings to  
 205 the BAM instrument during collocation at the Lawrenceville site after correction using a  
 206 hygroscopic growth factor only (i.e. corrected measurement is raw measurement divide by fRH).  
 207 Colors indicate relative humidity at the time of the measurements. Note that the NPM  
 208 measurement corrected in this manner severely underestimates PM<sub>2.5</sub> concentration. For PPA  
 209 sensors, while absolute errors are decreased relative to those of using the as-reported values  
 210 directly, bias is also increased and correlation is reduced.

Table S.42: Coefficients for empirical correction equations

Coefficient	Value Estimate	Standard Deviation	Unit
$\alpha_0$	0	2.9	$\mu\text{g}/\text{m}^3$
$\alpha_1$	2.93	0.08	N/A
$\alpha_2$	-0.11	0.08	$\mu\text{g}/^\circ\text{Cm}^3$
$\alpha_3$	0	0.08	$\mu\text{g}/\% \text{m}^3$
$\alpha_4$	$5.3 \times 10^{-4}$	$1.5 \times 10^{-4}$	$\text{m}^3/\mu\text{g}$
$\alpha_5$	$-8.9 \times 10^{-3}$	$1.2 \times 10^{-3}$	$^\circ\text{C}^{-1}$
$\alpha_6$	$-2.7 \times 10^{-2}$	$0.11 \times 10^{-2}$	$\%^{-1}$
$\alpha_7$	$2.9 \times 10^{-3}$	$0.8 \times 10^{-3}$	$\mu\text{g}/^\circ\text{C}^2 \text{m}^3$
$\alpha_8$	$5.0 \times 10^{-3}$	$1.0 \times 10^{-3}$	$\mu\text{g}/^\circ\text{C}\% \text{m}^3$
$\alpha_9$	0	$6.0 \times 10^{-4}$	$\mu\text{g}/\%^2 \text{m}^3$
$\beta_0$	75	11	$\mu\text{g}/\text{m}^3$
$\beta_1$	0.60	0.0090	N/A
$\beta_2$	-2.5	0.51	$\mu\text{g}/^\circ\text{Cm}^3$
$\beta_3$	-0.82	0.11	$\mu\text{g}/\% \text{m}^3$
$\beta_4$	2.9	0.53	$\mu\text{g}/^\circ\text{Cm}^3$
$\gamma_0$	21	2.1	$\mu\text{g}/\text{m}^3$
$\gamma_1$	0.43	0.013	N/A
$\gamma_2$	-0.58	0.090	$\mu\text{g}/^\circ\text{Cm}^3$
$\gamma_3$	-0.22	0.023	$\mu\text{g}/\% \text{m}^3$
$\gamma_4$	0.73	0.098	$\mu\text{g}/^\circ\text{Cm}^3$

212

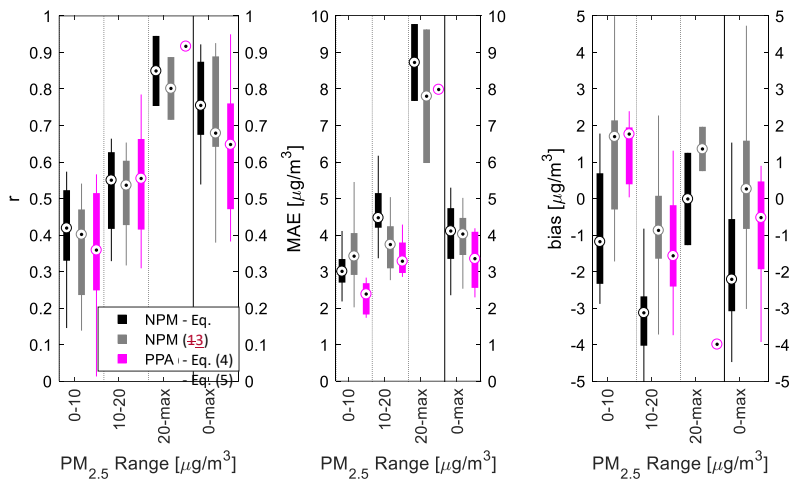
213 The following figure summarizes the medians and ranges in performance of the corrected NPM  
 214 and PPA hourly averaged data across both collocation sites, using all sensors deployed to both  
 215 sites (as opposed to only the testing set), as well as specifying performance by different  
 216 concentration ranges (0 to 10, 10 to 20, and higher than 20  $\mu\text{g}/\text{m}^3$ ). Correlation is typically better  
 217 for NPM sensors (using either empirical correction equation), with r between 0.7 and 0.9, while  
 218 for PPA sensors it ranges down to 0.5. Correlations also improve at higher concentrations. The  
 219 MAE for both sensors are between 3 and 5  $\mu\text{g}/\text{m}^3$ . MAE also tends to increase as concentrations  
 220 increase, but the PPA sensors appear to be less affected than NPM at concentrations above 20  
 221  $\mu\text{g}/\text{m}^3$ ; however, considering there were only two PPA sensors at the Lincoln site (where these  
 222 higher concentrations were more common) this may be a sample size artefact. Although unbiased  
 223 over the full range, the corrected sensor readings tend to be positively biased at low  
 224 concentrations and negatively biased at moderate concentrations. This is opposite to the trend  
 225 seen before correction and may be due to overcorrections at the extremes.



227

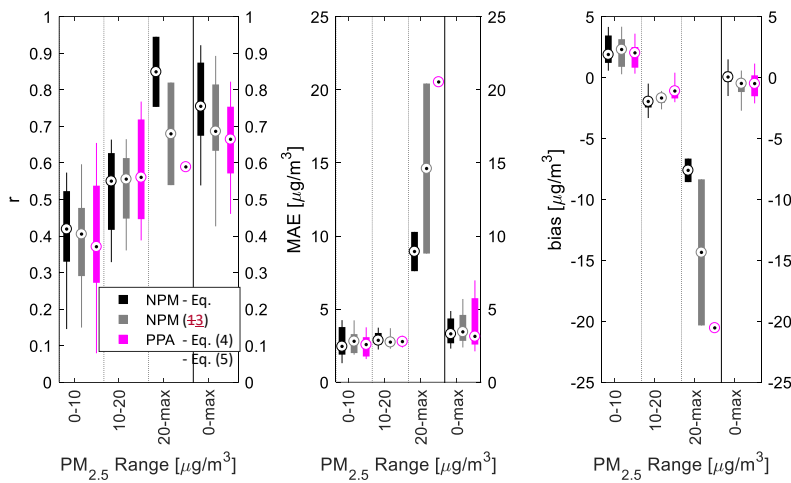
228 Figure S.107: Comparison of one-hour-average corrected sensor performance compared to BAM  
 229 instruments during collocation at both the Lawrenceville and Lincoln sites. Performance metrics  
 230 are plotted overall (0-max range) and by different PM<sub>2.5</sub> ranges (0-10, 10-20, 20-max). Results  
 231 shown relate to a total of 32 NPM and 11 PPA sensors, and only consider sensors with at least  
 232 five samples in the relevant range.

233 The following figures illustrate how the performance of the proposed correction approaches is  
 234 affected if data from just one of the sites (Lincoln or Lawrenceville) is used to train the model,  
 235 and it is then tested on data from the other site.



236

237 Figure S.11: Comparison of sensor performance compared to the BAM instrument during  
 238 collocation at the Lawrenceville site, using correction models calibrated using only data  
 239 collected at the Lincoln site. Performance is comparable in terms of correlation and MAE to  
 240 models trained using data from both sites, although bias, especially using Eq. (3) for NPM  
 241 sensors, is generally worse.



242

243 Figure S.12: Comparison of sensor performance compared to the BAM instrument during  
 244 collocation at the Lincoln site, using correction models calibrated using only data collected at the  
 245 Lawrenceville site. Performance is comparable except in the 20-max range, where performance

246 is significantly worse than for models calibrated using data from both sites. This illustrates the  
 247 importance of calibrating correction equations across the entire range of concentrations which  
 248 might be expected during field deployments.

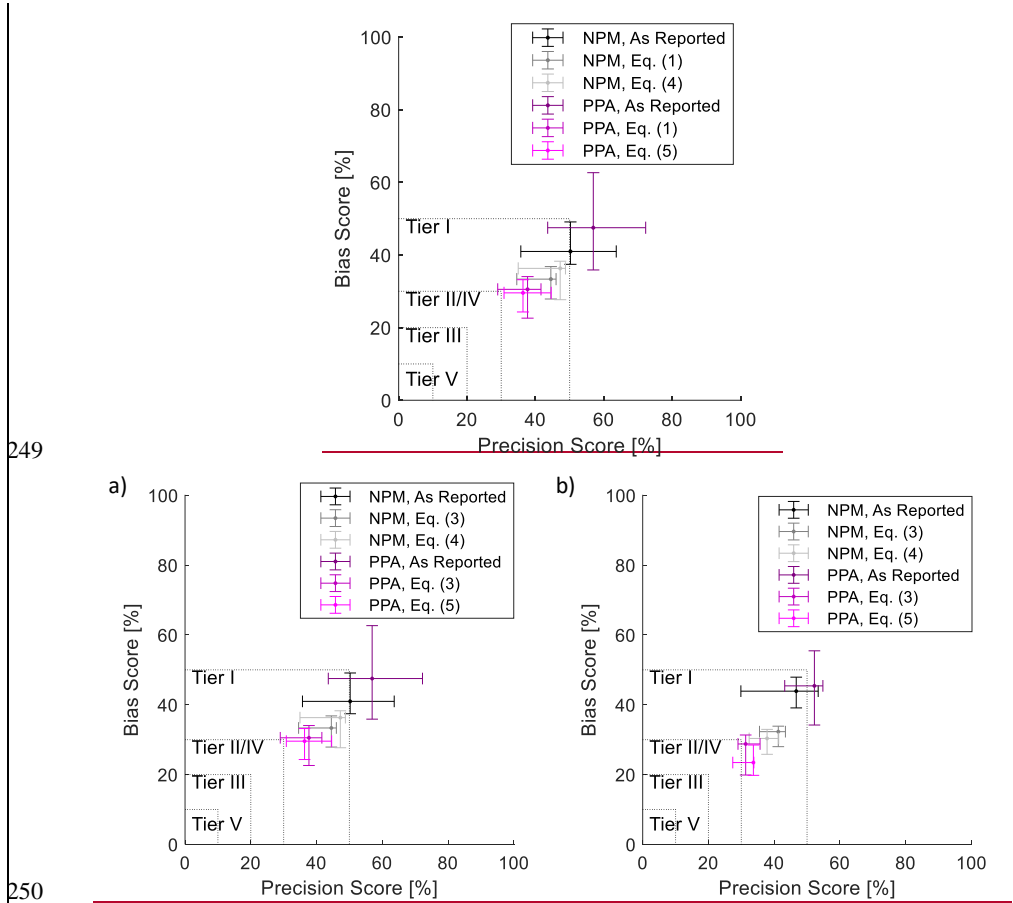
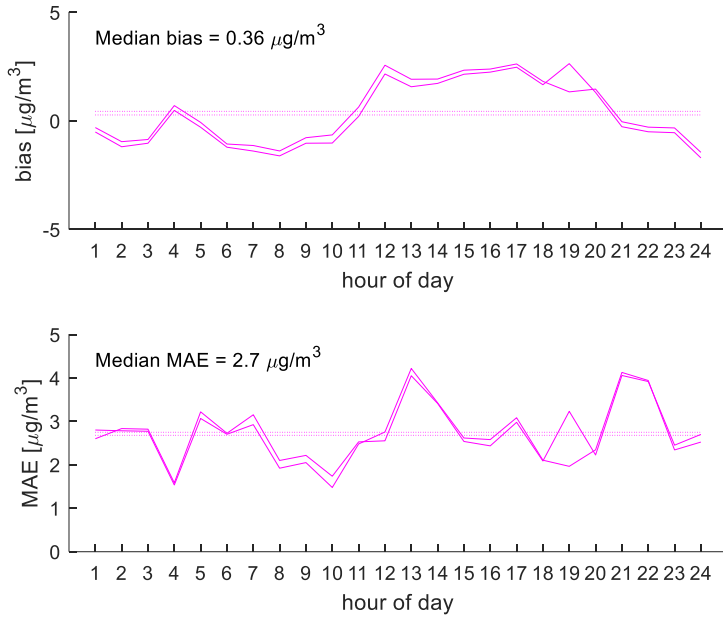


Figure S.1340: Evaluation of EPA precision and bias score metrics for hourly-averaged (a) or daily-averaged (b) data from NPM and PurpleAir sensors. Center-points of crosses indicate median performance, with arms indicating 25%-75% range. Following corrections, both instruments meet Tier I requirements for educational and informational monitoring.



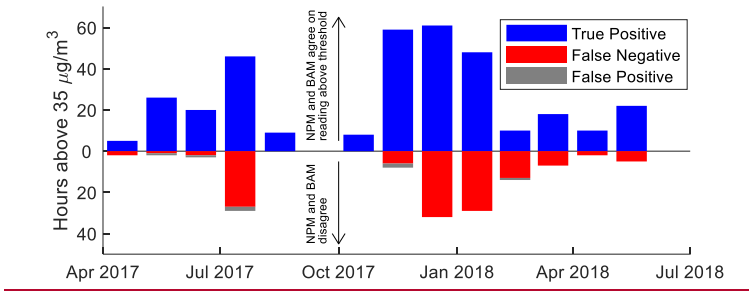
255

256

257 Figure S.14: Results of a performance evaluation of a pair of PurpleAir sensors at the Parkway  
 258 East site. Corrections are performed using Eq. (3). Results cover a data collection period of three  
 259 weeks. Hourly-average bias and MAE are plotted as a function of time of day in the solid lines  
 260 for the two sensors; dotted lines indicate the median performance throughout the day for each  
 261 sensor. Median bias and MAE for both sensors are also listed in the figure. Corrections are  
 262 performed using Eq. (1).

263 **S.8. Short-Term Performance Assessment**

Formatted: Heading 1



264

265 Figure S.15: Detection of hourly high  $\text{PM}_{2.5}$  events by NPM sensor at Lincoln. True positives  
 266 (correct detections) are counted for each hour on a monthly basis, along with false positives

267 (NPM falsely indicated high PM) and false negatives (NPM missed high PM), with a grace  
268 period of ±1 hour.

269

270 Camalier L, Eberly S, Miller J, Papp M. 2007. Guideline on the Meaning and the Use of  
271 Precision and Bias Data Required by 40 CFR Part 58 Appendix A.

272 Cerully KM, Bougiatioti A, Hite JR, Guo H, Xu L, Ng NL, et al. 2015. On the link between  
273 hygroscopicity, volatility, and oxidation state of ambient and water-soluble aerosols in  
274 the southeastern United States. Atmospheric Chemistry and Physics 15:8679–8694;  
275 doi:10.5194/acp-15-8679-2015.

276 Gu P, Li HZ, Ye Q, Robinson ES, Apte JS, Robinson AL, et al. 2018. Intra-city variability of PM  
277 exposure is driven by carbonaceous sources and correlated with land use variables.  
278 Environmental Science & Technology; doi:10.1021/acs.est.8b03833.

279 Jayaratne R, Liu X, Thai P, Dunbabin M, Morawska L. 2018. The influence of humidity on the  
280 performance of a low-cost air particle mass sensor and the effect of atmospheric fog.  
281 Atmospheric Measurement Techniques 11:4883–4890; doi:10.5194/amt-11-4883-2018.

282 Johnson KK, Bergin MH, Russell AG, Hagler GSW. 2016. Using Low Cost Sensors to Measure  
283 Ambient Particulate Matter Concentrations and On-Road Emissions Factors.  
284 Atmospheric Measurement Techniques Discussions 1–22; doi:10.5194/amt-2015-331.

285 Petters MD, Kreidenweis SM. 2007. A single parameter representation of hygroscopic growth  
286 and cloud condensation nucleus activity. Atmospheric Chemistry and Physics 7:1961–  
287 1971; doi:10.5194/acp-7-1961-2007.

288 Saha PK, Robinson ES, Shah RU, Zimmerman N, Apte JS, Robinson AL, et al. 2018. Reduced  
289 Ultrafine Particle Concentration in Urban Air: Changes in Nucleation and Anthropogenic  
290 Emissions. Environmental Science & Technology 52:6798–6806;  
291 doi:10.1021/acs.est.8b00910.

292 Saha PK, Zimmerman N, Malings C, Haurlyuk A, Li Z, Snell L, et al. 2019. Quantifying high-  
293 resolution spatial variations and local source impacts of urban ultrafine particle  
294 concentrations. Science of The Total Environment 655:473–481;  
295 doi:10.1016/j.scitotenv.2018.11.197.

296 Schmidt M, Lipson H. 2009. Distilling Free-Form Natural Laws from Experimental Data.  
297 Science 324:81–85; doi:10.1126/science.1165893.

298 Stanier CO, Khlystov AY, Pandis SN. 2004. Ambient aerosol size distributions and number  
299 concentrations measured during the Pittsburgh Air Quality Study (PAQS). Atmospheric  
300 Environment 38:3275–3284; doi:10.1016/j.atmosenv.2004.03.020.

Formatted: Indent: Left: 0.04"

Formatted: Bibliography, Widow/Orphan control, Adjust space between Latin and Asian text, Adjust space between Asian text and numbers

Field Code Changed

